# Finite-size and nonlinear effects on the ultrafast electron transport in thin metal films

G. Manfredi and P.-A. Hervieux
*Institut de Physique et Chimie des Matériaux de Strasbourg, GONLO, BP 43, F-67034 Strasbourg, France*
(Received 4 February 2005; revised manuscript received 23 June 2005; published 18 October 2005)

Self-consistent simulations of the electron dynamics and transport in thin metal films are performed using a semiclassical Vlasov-Poisson model. The Vlasov equation is solved using an accurate Eulerian scheme that preserves the fermionic character of the electron distribution. Although the thermodynamical properties of the ground state are accurately described by the bulk theory, the dynamical properties are strongly influenced by the finite size of the system and the presence of surfaces. Our results show that (i) heat transport is ballistic and occurs at a velocity close to the Fermi speed; (ii) after the excitation energy has been absorbed by the film, slow nonlinear oscillations appear, with a period proportional to the film thickness, which are attributed to nonequilibrium electrons bouncing back and forth on the film surfaces; (iii) except for trivial scaling factors, the above transport properties are insensitive to the excitation energy and the initial electron temperature. Finally, the coupling to the ion dynamics and the impact of electron-electron collisions are also investigated.

DOI: 10.1103/PhysRevB.72.155421 PACS number(s): 73.50.−h, 73.22.−f, 78.47.+p

## I. INTRODUCTION

The ultrafast electron dynamics in optically excited metallic nanostructures is of great importance for both fundamental studies and technological applications in materials science. Thin metal films of submicron thickness are typical examples of nanostructures and are widely used in modern high-speed electronic and optoelectronic devices. In such systems, the switching time can nowadays approach the femtosecond time domain. On this time scale, the electron distribution is out of thermal equilibrium. In order to control the energy consumption, it is therefore important to develop a better understanding of electron transport and energy relaxation in the femtosecond temporal regime.

Due to the presence of interfaces, the ion and electron dynamics in finite-size metallic nanostructures display unexpected features. For example, as the elastic and inelastic-scattering length ($\sim$10–50 nm for bulk metals) are much longer than the size of the system, an electron—or a group of electrons—can travel coherently through the length of the system, thus leading to ballistic transport between the surfaces. On a longer time scale, the transport generally becomes diffusive due to electron-electron, electron-surface, and electron-ion collisions.

Experimentally, thanks to the recent development of ultrafast spectroscopy techniques, it is now possible to monitor the femtosecond dynamics of an electron gas confined in metallic nanostructures such as thin films,[1–8] nanotubes,[9] metal clusters,[10,11] and nanoparticles.[6,7,12,13] Therefore, meaningful comparisons between experimental measurements and numerical simulations based on microscopic theories are becoming possible.

From the theoretical point of view, a number of phenomenological models[2,14–20]—originally developed for bulk materials—employ Boltzmann-type equations within the framework of Fermi-liquid theory.[21] However, such approaches fail to describe finite-size systems because the interfaces, which play a crucial role in the ultrafast dynamics, are not included.

To our knowledge, few comprehensive investigations based on microscopic models (either quantal or semiclassical) are available in the literature. Concerning quantal models, ultrafast electron dynamics in metal clusters was investigated by Calvayrac *et al.*[22] using time-dependent density functional theory, both in the linear and nonlinear regimes. The many-particle quantum dynamics of the electron gas in a thin metal film was studied by Schwengelbeck *et al.*[23] within the time-dependent Hartree-Fock approximation. However, due to their considerable computational cost, these approaches are limited to relatively small systems.

The semiclassical limit of the previous quantal approaches is given by the self-consistent Vlasov-Poisson system. The Vlasov-Poisson model was used to perform particle-in-cell (PIC) simulations of the electron dynamics in metal clusters,[22,24] and to obtain analytical results in the linear regime for metal clusters[25] and thin films.[26] The PIC method consists in approximating the distribution function with a finite number of pseudoparticles. A major disadvantage of PIC simulations applied to Fermi systems is the loss of the fermionic character of the distribution as time evolves. This spurious effect is due to the numerical noise inherent to the PIC method, which is too large to allow a precise description of the phase space.

The purpose of the present work is to present extensive computational results on the ultrafast dynamics of electrons and ions in thin metal films, obtained using a very accurate and stable numerical method for the semiclassical Vlasov-Poisson system. The Vlasov equation is solved on a regular phase-space mesh using a Eulerian code,[27] which is not based on discrete particles such as PIC codes and thus displays a very low level of numerical noise. Most importantly for metallic nanostructures, the Eulerian code preserves the fermionic character of the electron distribution at all times. Our numerical results provide clear evidence for the important role played by the finiteness of the system on the electron dynamics and transport. In particular, the presence of surfaces is shown to influence crucially the process of electron thermalization.

The experimental setup we have in mind for our simulations is that of a typical pump-probe experiment. In this situation, the following schematic scenario is generally assumed: first, the electrons absorb quasi-instantaneously the laser en-

 

ergy via interband and/or intraband transitions (the establishment of the polarization is instantaneous in a Poisson model since no retardation effects are included). Under certain conditions (e.g., not too high energy transfer[28]) this early stage leads to the creation of a collective oscillation, the so-called surface or volume plasmon. Subsequently, the plasmon oscillation is damped through coupling to self-consistent quasiparticle excitations[29,30] (Landau damping). This damping occurs on a very fast time scale ($<10$ fs): it was observed experimentally in gold nanoparticles[31] and was studied theoretically in several works.[26,30,32] During these fast processes, the ionic background remains frozen and the electron distribution is nonthermal. As a result, the electron temperature cannot be properly defined at this stage of the relaxation process.

On a longer time scale ($>10$ fs), the injected energy is redistributed among the electrons via electron-electron collisions, leading to the so-called "internal" electron thermalization. Electron-lattice ("external") thermalization was generally supposed to occur on even longer time scales. However, the results of Refs. 5 and 14 on thin gold films have shown that nonequilibrium electrons start interacting with the lattice earlier than expected, so that a clear separation between internal and external relaxation is not entirely pertinent.

Other experiments have measured the properties of heat transport in thin gold films,[1,2] showing that it is not a diffusive process (Brownian motion), but rather a ballistic one (motion at constant velocity). These works demonstrated that heat transport occurs on a femtosecond time scale and involves nonequilibrium electrons travelling at a velocity close to the Fermi velocity of the metal.

In the present work, we perform Vlasov-Poisson simulations to study the relaxation processes described in the above paragraphs. Preliminary results on this problem were presented in a previous paper.[33] The self-consistent Vlasov-Poisson model is described in detail in Sec. II, whereas Sec. III is devoted to the description of the numerical method. In Sec. IV, the ground-state properties of the films are investigated. The numerical results on the ultrafast dynamics and transport are shown in Sec. V (for the electrons) and Sec. VI (for the electron-ion coupling). The impact of electron-electron collisions is investigated in Sec. VII. Finally, Sec. VIII contains a critical discussion of the results and some hints at possible future developments of the present work.

## II. VLASOV-POISSON MODEL

The electron dynamics in metallic nanostructures (including thin metal films) is often described through quantum mean-field models, such as the time-dependent Hartree equations. Mean-field models take into account collective effects due to the global electric charge and current distributions, but neglect two-body correlations (i.e., binary collisions). This is a fairly reasonable assumption for highly degenerate electron gases in metallic nanostructures at room temperature, as the exclusion principle forbids a vast number of transitions that would otherwise be possible[34] (this effect is known as "Pauli blocking"). Consequently, the electron mean-free-path is often larger than the size of the system. For instance, for the sodium films considered in this work, the bulk mean-free-path is about 34 nm, whereas the film thickness varies in the range 10–30 nm. In addition, there is a conceptual advantage in isolating a single physical mechanism (the mean field), insofar as the observed results can be unambiguously ascribed to that very mechanism.

In the semiclassical limit, the electron dynamics can be described by the Vlasov equation[22]

$$\frac{\partial f_e}{\partial t} + v_x \frac{\partial f_e}{\partial x} + \frac{e}{m_e}\frac{\partial \phi}{\partial x}\frac{\partial f_e}{\partial v_x} = 0, \tag{1}$$

coupled self-consistently to Poisson's equation for the electrostatic potential (magnetic fields will be ignored throughout this work)

$$\frac{\partial^2 \phi}{\partial x^2} = -\frac{e}{\varepsilon_0}[n_i(x) - n_e(x,t)], \tag{2}$$

where $n_e = \int_{-\infty}^{+\infty} f_e dv_x$. We have further assumed that the singly charged ions form a motionless neutralizing background with inhomogeneous density

$$n_i(x) = \frac{n_0}{1 + e^{(|x|-L/2)/\sigma_i}}, \tag{3}$$

where $n_0$ is the ion density of the bulk metal and $\sigma_i$ a diffuseness parameter[22] (simulations with mobile ions will be reported in Sec. VI).

The one-dimensional (1D) approximation used in Eqs. (1)–(3) relies on the fact that a thin film can be viewed as an infinite slab of thickness $L$. This assumption holds if the film size in the directions parallel to its surfaces is large compared to $L$. In this case, it is appropriate to use a 1D model, where only the normal coordinate $x$ and its corresponding velocity $v_x$ play a role. Accordingly, the electric field is normal to the film surfaces and only volume modes in the electron dynamics can be studied, whereas surface modes are neglected (for further details, see the introductory paragraph of Sec. V).

The Vlasov-Poisson equations (1)–(2) constitute a nonlinear self-consistent system, as the electric potential determines $f_e$ in Eq. (1) and is in turn determined by it in Eq. (2). This model will be used throughout the present paper to describe the electron dynamics in a thin metal film.

The system (1)–(2) must of course be supplemented with boundary and initial conditions. For the electron distribution, we define a computational box: $-L_{\max}/2 \leqslant x \leqslant L_{\max}/2$ and $-V_{\max} \leqslant v_x \leqslant V_{\max}$, with $L_{\max} \gg L$ and $V_{\max} \gg v_F$, where $v_F$ is the Fermi velocity of the metal. We then assume that $f(x, v_x = \pm V_{\max}, t) = 0$ and $f(x = L_{\max}/2, v_x < 0, t) = f(x = -L_{\max}/2, v_x > 0, t) = 0$. The latter equality amounts to imposing zero incoming flux at the $x$ boundaries of the computational box. The boundary conditions on the electrostatic potential will be described shortly.

Concerning the initial condition, it is reasonable to assume that the electrons are at thermodynamic equilibrium with a certain temperature $T_e$. At room temperature, $T_e$ is generally much smaller than the Fermi temperature $T_F$, so that the relevant equilibrium is given by the quantum Fermi-

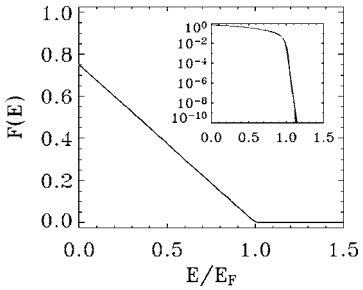


FIG. 1. Energy distribution function at $t=0$ and $\omega_{pe}t=1000$ for a case without perturbation. The inset shows a semilog plot of the same curve. Virtually no variation in the distribution can be detected. The film thickness and temperature are, respectively, $L=100L_F$ and $T_e=0.008T_F$.

Dirac distribution. In this sense, our model can be referred to as semiclassical (classical dynamics, but quantum statistics at equilibrium).

As was mentioned above, it is appropriate to use a 1D infinite slab geometry to describe the electron dynamics in the film. However, at thermodynamic equilibrium, the electrons should be allowed to occupy all available states in velocity space, and there is no reason why states with $v_y \neq 0$ and $v_z \neq 0$ should be unoccupied. Therefore, even in 1D geometry, the equilibrium distribution should always be described by a three-dimensional (3D) Fermi-Dirac function,

$$f_{e0}^{\mathrm{3D}}(x,\mathbf{v}) = \mathrm{const} \times \frac{1}{1+e^{\beta_e(\epsilon-\mu)}}, \tag{4}$$

where $\beta_e=1/k_BT_e$, $\mu$ is the chemical potential, and $\epsilon=m|\mathbf{v}|^2/2-e\phi(x)$ is the local single-particle energy (here, $\mathbf{v}$ is the 3D velocity vector).

However, it is still possible to keep the 1D geometry for the Vlasov-Poisson system, provided that one uses, as initial condition, the 3D Fermi-Dirac distribution (4) projected on the $v_x$ axis, $f_{e0}(x,v_x)=\int\int f_{e0}^{\mathrm{3D}}dv_ydv_z$. This integral can be performed analytically and yields (restoring the correct multiplicative constant)

$$f_{e0}(x,v_x) = \frac{3}{4}\frac{n_0}{v_F}\frac{T_e}{T_F}\ln(1+e^{-\beta_e(\epsilon-\mu)}), \tag{5}$$

with $\epsilon(x,v_x)=mv_x^2/2-e\phi(x)$. Note that, at zero temperature, the above expression becomes linear in the energy (see Fig. 1),

$$f_{e0}^{T_e=0}(x,v_x) = \frac{3}{4}\frac{n_0}{v_F}\left(1-\frac{\epsilon}{E_F}\right) \quad \text{for } |v_x| \leqslant v_F \tag{6}$$

and $f_{e0}^{T_e=0}=0$, for $|v_x|>v_F$.

In order to obtain the equilibrium distribution, Eq. (5) is inserted into Poisson's equation (2), which becomes a nonlinear equation for $\phi(x)$ that can be solved numerically using an iterative procedure. Once the electric potential $\phi(x)$ has been computed, it can be substituted back into Eq. (5) to obtain the initial equilibrium state. The nonlinear Poisson's equation is solved with boundary conditions $\phi'(-L_{\max}/2)=\phi'(L_{\max}/2)=0$ (the apex denotes the $x$ derivative), which corresponds to zero electric field at the boundaries. By integrating Eq. (2) on the interval $[-L_{\max}/2, L_{\max}/2]$, it is easy to see that these boundary conditions imply that the total electric charge in the computational box vanishes, i.e., $\int n_e dx = \int n_i dx$.

It must be added that one cannot use the same boundary conditions on the Poisson's equation during the time evolution. Indeed, in this case the electron density $n_e$ is an independent variable and no longer a function of $\phi$. Therefore, the total electric charge cannot be forced *a priori* to be equal to zero (because, in principle, some electrons could have left the computational box). Our strategy is to use Dirichlet boundary conditions $\phi(\pm L_{\max}/2,t)=0$ during the evolution and to choose $L_{\max}$ large enough so that virtually no electrons leave the computational box.

Finally, it is convenient to express all quantities in terms of a few normalized units that represent typical velocity, time and length scales for a self-consistent electron gas. This amounts to normalizing time to the inverse of the plasmon frequency $\omega_{pe}=(e^2n_0/m_e\varepsilon_0)^{1/2}$, velocity to the Fermi speed $v_F$, and length to $L_F=v_F/\omega_{pe}$; in addition, particle densities are normalized to the ion density of the bulk metal $n_0$. For alkali metals we have $L_F=0.59(r_s/a_0)^{1/2}$ Å, $\omega_{pe}^{-1}=1.33\times10^{-2}(r_s/a_0)^{3/2}$ fs, $E_F=50.11(r_s/a_0)^{-2}$ eV, and $T_F=5.82\times10^5(r_s/a_0)^{-2}$ K, where $r_s$ is the Wigner-Seitz radius. For sodium, $r_s=4a_0$ with $a_0=0.529$ Å. The ion plasmon frequency $\omega_{pi}=(e^2n_0/m_i\varepsilon_0)^{1/2}$ is much larger than $\omega_{pe}$, due to the large ion-to-electron mass ratio. In our case, we have that the electron and ion plasmon periods (defined as $2\pi/\omega_p$) are, respectively, 0.67 fs ($\approx 6.28\ \omega_{pe}^{-1}$) and 137.68 fs ($\approx 1300\ \omega_{pe}^{-1}$). The simulations with fixed ions are equivalent to assuming $m_i\to\infty$ and thus $\omega_{pi}\to 0$.

## III. NUMERICAL METHOD

In this work, we shall present computational results obtained from the numerical resolution of the Vlasov-Poisson system (1)–(2). The standard technique to solve this system is the so-called particle-in-cell (PIC) method, according to which the electron distribution is represented as a sum of delta functions, $f_e(x,v_x,t)=\Sigma_{j=1}^{N} w_j\delta(x-x_j(t))\delta(v-v_{xj}(t))$, where the $w_j$ are constant weights, and $x_j$ and $v_{xj}$ are the position and velocities of $N$ test-particles obeying the classical equations of motion (characteristics of the Vlasov equation), $\dot{x}_j=v_{xj}$ and $m_e\dot{v}_{xj}=-eE(x_j)$. The electric field $E=-\partial\phi/\partial x$ is computed by projecting the particle density on a spatial mesh and then solving Poisson's equation.

For applications to degenerate electron plasmas, this method presents at least two drawbacks: (i) In the initial state, the particles are loaded at random so that some statistical noise is introduced, which will pollute the simulation results at all subsequent times. Statistical noise is proportional to $N^{-1/2}$, and is therefore difficult to eliminate by simply increasing the number of particles;[35] (ii) More importantly, PIC methods violate the exclusion principle,[36] so that the initial Fermi-Dirac equilibrium quickly relaxes to a Maxwell-Boltzmann distribution (this relaxation is caused by the very same statistical noise mentioned above). The accu-

racy of PIC simulations can be improved by using finite-size particles (i.e., replacing the Dirac delta functions with smoother functions)[37] or by introducing *ad hoc* collision operators.[38] Nevertheless, Maxwell-Boltzmann thermalization is still observed after some time. In addition, these corrections make it difficult to separate the collisionless Vlasov dynamics from the effect of such *ad hoc* terms.

In contrast, Eulerian codes solve the Vlasov equation using standard methods developed for parabolic partial differential equations.[27,39,40] The entire phase space $(x,v_x)$ is covered with a regular mesh and the distribution function is defined on the mesh nodes (nonuniform meshes have also been proposed,[41] but will not be used here). As a result, Eulerian codes display very low numerical noise (even in regions where the electron gas is rarefied, which is where PIC codes would be most noisy) and are capable of preserving the fermionic character of the distribution function for extremely long times. The latter property is crucial to obtain meaningful simulation results for a degenerate electron gas. It must be said that Eulerian codes do require a larger computational effort, both in terms of computing time and storage memory, particularly for fully 3D problems, which require the meshing of a six-dimensional (6D) phase space. Today's computing facilities, however, tend to make these limitations somewhat less relevant.

In order to illustrate the good properties of Eulerian codes, we have prepared the system in a Fermi-Dirac equilibrium at low temperature ($T_e/T_F=0.008$) and then let it evolve following the Vlasov-Poisson system. In this example, the film has thickness $L=100L_F$ and the ions are kept fixed. By definition, this Fermi-Dirac equilibrium is a stationary solution of the Vlasov equation (indeed, all functions of the energy only are) and therefore should not change in time. The stability of this initial condition was verified by monitoring the energy distribution $f(E,t)$, obtained by averaging $f_e(x,v_x,t)$ over surfaces at constant energy

$$f(E,t)=\frac{\int\int f_e(x,v_x,t)\,\delta(\epsilon(x,v_x,t)-E)dxdv_x}{\int\int \delta(\epsilon(x,v_x,t)-E)dxdv_x}, \qquad (7)$$

where $\epsilon(x,v_x)$ is the single-particle energy defined in Sec. II, $\delta$ is the Dirac delta function, and the integration is over the entire phase space. Figure 1 shows the energy distribution at times $t=0$ and $\omega_{pe}t=1000$. The two curves are virtually indistinguishable on the scale of the figure (even on a semilog scale down to very small amplitudes), confirming the very good stability of our Eulerian code. Over the entire simulation, the total energy is conserved within an error of less than 0.05%. In contrast, PIC codes show a rapid deterioration of the Fermi-Dirac ground state, which relaxes to a Boltzmann distribution in about 13 electron plasmon cycles ($\omega_{pe}t\simeq 80$ in our units).[37,38] We conclude that the use of Vlasov Eulerian codes is an effective method to preserve Pauli's exclusion principle during the semiclassical evolution of the electron system.

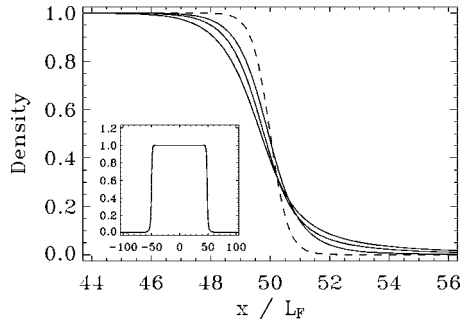


FIG. 2. Density profile (normalized to $n_0$) near the surface, for a film with $L=100L_F$, $\sigma_i=0.3L_F$, and electron temperatures $T_e/T_F=0.03$, 0.5, and 1.0 (the steeper curves have lower temperatures). The dashed line represents the ion density profile. The inset shows the electron density over the entire film.

## IV. GROUND STATE

Before attacking the more challenging study of the electron dynamics and transport, it is useful to investigate the properties of the self-consistent ground state. As detailed in Sec. II, this is obtained numerically by solving the nonlinear Poisson equation (2), with the electron distribution given by Eq. (5). Three cases were analyzed in detail, (i) $L=100L_F$ and $\sigma_i=0.3L_F$; (ii) $L=200L_F$ and $\sigma_i=0.3L_F$; and (iii) $L=200L_F$ and $\sigma_i=L_F$. For each case, several calculations were performed for different temperatures, ranging from $T_e=0.003T_F$ to $T_e=T_F$. The results were compared to those predicted by the thermodynamical theory of an infinite system of noninteracting fermions (Fermi gas).

Typical profiles for the ground state are shown in Figs. 2 and 3 for the parameters of case (i) and different temperatures. The "spill out" of the electron density (with respect to the ion density) is visible even for $T_e\ll T_F$ and increases with the temperature. The potential profile is flat inside the film and displays a steep jump at the two surfaces.

Several energy quantities were considered (all normalized to the Fermi energy). The total energy of the electron gas is given by the sum of kinetic plus potential energy, $E_{\rm tot}=E_{\rm kin}+E_{\rm pot}$. Further, the kinetic energy can be split into two parts, the Thomas-Fermi energy (energy of the equivalent zero-temperature state with same density) $E_{\rm TF}=\frac{1}{5}\int n_e(x)^{5/3}dx$ and the thermal energy $E_{\rm th}=E_{\rm kin}-E_{\rm TF}$. The thermal energy corresponds to the kinetic energy of the electrons located in a shell of thickness $k_BT_e$ around the Fermi surface. The ther-

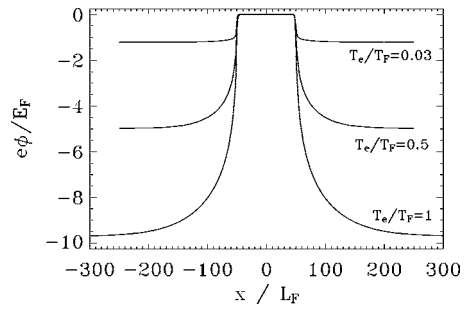


FIG. 3. Electric potential profile for a film with $L=100L_F$, $\sigma_i=0.3L_F$, and electron temperatures $T_e/T_F=0.03$, 0.5, and 1.0.

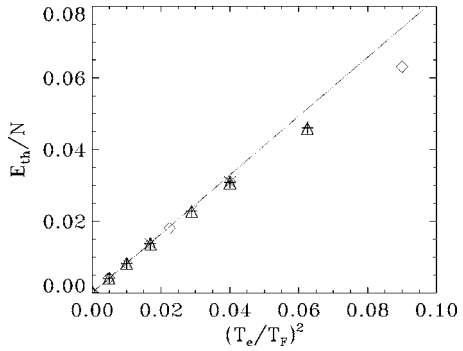


FIG. 4. Thermal energy per particle as a function of the squared electron temperature, for three cases, $L=100L_F$ and $\sigma_i=0.3L_F$ (diamonds); $L=200L_F$ and $\sigma_i=0.3L_F$ (triangles); and $L=200L_F$ and $\sigma_i=L_F$ (stars). All energies are normalized to $E_F$. The continuous line represents the theoretical result for the bulk at low temperatures.

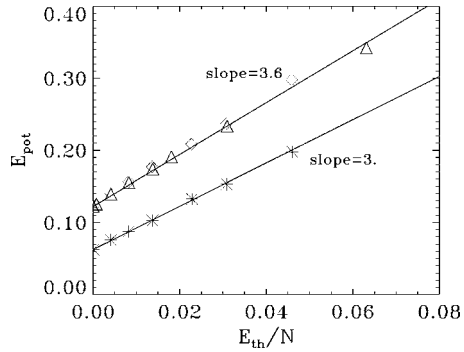


FIG. 6. Potential energy versus thermal energy per particle, for three cases, $L=100L_F$ and $\sigma_i=0.3L_F$ (diamonds); $L=200L_F$ and $\sigma_i=0.3L_F$ (triangles); and $L=200L_F$ and $\sigma_i=L_F$ (stars). All energies are normalized to $E_F$. The straight lines are fits to the numerical data.

mal energy *per particle* $\bar{E}_{\rm th}$ is obtained by dividing $E_{\rm th}$ by the normalization of $f_e(x,v_x)$, which is $N=\int\int f_e dx dv_x$.

Figure 4 shows the thermal energy per particle as a function of the square of the electron temperature. The theoretical estimate for an infinite Fermi gas at low temperature yields $\bar{E}_{\rm th}=C(T_e/T_F)^2$, with $C=\pi^2/12\simeq 0.82$, which fits very well the numerical results.[42]

In Eq. (5), there is a certain ambiguity on the value of the chemical potential $\mu$, as the electric potential $\phi(x)$ is defined up to an additive constant, which can be attached either to $\phi$ or to $\mu$. We choose this constant in such a way that the chemical potential is directly comparable to its definition in the bulk, where $\phi\equiv 0$. Therefore, we impose that the electric potential is equal to zero in the center of the film, where the effect of the surfaces is negligible (see Fig. 3). Once this constant is fixed, the value of $\mu$ is then unambiguously determined. The value of $\mu$ is plotted in Fig. 5 for the three cases defined above and several values of $T_e$. The numerical computations reproduce very accurately the exact theoretical result (valid for all temperatures) obtained for noninteracting bulk fermions in three dimensions.

From the results of Figs. 4 and 5, it is clear that the thermodynamical properties of the electron gas in the film are mainly those of an infinite noninteracting fermion gas (at least for our semiclassical model; deviations from bulk behavior were recently observed in a quantal model[43]). The

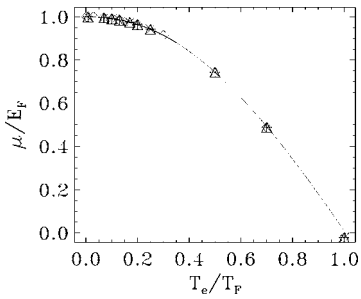


FIG. 5. Chemical potential as a function of the electron temperature, for three cases, $L=100L_F$ and $\sigma_i=0.3L_F$ (diamonds); $L=200L_F$ and $\sigma_i=0.3L_F$ (triangles); and $L=200L_F$ and $\sigma_i=L_F$ (stars). The continuous line represents the theoretical result for the bulk.

finiteness of the system and the presence of strong self-consistent electric fields at the surfaces do not seem to play a significant role. This is far from trivial, as the dynamical properties of the electron gas (see next section) will turn out to be mainly determined by the very presence of electrically charged surfaces. The lesson to be learned is that the fact that bulk theory works well for the ground state is no guarantee that it will succeed in time-dependent situations.

In order to investigate the ground state properties that depend crucially on the finiteness of the system, we need to monitor quantities that involve the potential (i.e., electric) energy, $E_{\rm pot}=\varepsilon_0/2\int E^2 dx$. An interesting result is obtained by plotting the potential energy versus the thermal energy per particle (Fig. 6). For a wide range of temperatures, we observe a linear relationship between $E_{\rm pot}$ and $\bar{E}_{\rm th}$, with the potential energy taking a finite value as $T_e\to 0$. By varying the system size, the points fall on the same straight line, showing that this linear relationship is size independent. Taking a larger value of $\sigma_i$ (which determines the ion density profile at the surfaces), the points still fall on a straight line with lower potential energy, although the slope is slightly different.

Another interesting quantity is the electric potential jump between the center of the film ($x=0$) and a point far from the film surface, $\Delta\phi=\phi(0)-\phi(L_{\rm max})$ (Fig. 7). $e\Delta\phi$ represents the energy needed to bring an electron (initially at rest) from the center of the film to a point far away from it. At zero electron temperature, $e\Delta\phi$ is obviously equal to the Fermi energy. At finite temperature, $e\Delta\phi$ increases linearly with $T_e$; this linear relationship is very well verified up to $T_e\simeq 0.5T_F$. The quantity $e\Delta\phi$ also represents the energy of the phase-space separatrix that discriminates between bound electrons (with energies $\varepsilon<e\Delta\phi$) and unbound electrons ($\varepsilon>e\Delta\phi$).

The fact that $e\Delta\phi$ increases with the temperature may seem surprising, as one would rather imagine that it is easier to extract an electron from a warmer, rather than colder, electron gas. The caveat comes from the self-consistency: when $T_e$ is increased (keeping the ion profile fixed), the electron density becomes smoother at the surfaces, yielding a larger charge separation, which in turn increases the electric field and the potential jump at the surfaces. In other words, one

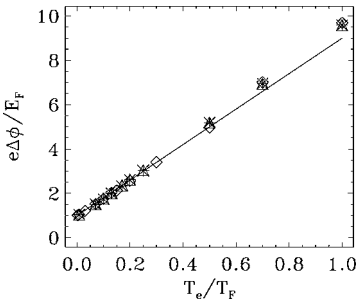


FIG. 7. Electric potential jump over the film extension versus the electron temperature, for three cases, $L=100L_F$ and $\sigma_i=0.3L_F$ (diamonds); $L=200L_F$ and $\sigma_i=0.3L_F$ (triangles); and $L=200L_F$ and $\sigma_i=L_F$ (stars). The straight line (with a slope equal to 8.0) is a fit to the numerical data.

cannot increase the electron temperature without altering the electric potential profile, as was already obvious from the results of Fig. 6. Nonetheless, one should keep in mind that $e\Delta\phi$ is the energy needed to extract an electron *at rest* (i.e., $v_x=0$). Obviously, electrons with a finite velocity will need a lesser amount of energy. For an electron gas at finite temperature, although the potential jump is indeed larger, there are actually more electrons with higher velocities that can be easily extracted.

## V. DYNAMICS AND TRANSPORT

In order to study the electron dynamics, a small perturbation was added to the electronic ground state. The perturbation was in the form of a uniform shift $\delta v$ of the entire electron population in velocity space.[22] In this way, an amount of energy is injected into the system in the form of kinetic energy of the center of mass of the electron population. After applying such perturbation, the electron gas is left to evolve under the action of the self-consistent electric potential.

We consider situations where no linear momentum is transferred parallel to the plane of the surface (i.e., only excitations with $q_\parallel=0$ are taken into account). This situation corresponds to the excitation of the slab with optical pulses[44] and also to the response to a uniform electric field oriented normal to the surface. The dispersion relation of the slab collective modes is given by the well-known expression[45] $\omega_\pm(q_\parallel)=\omega_{pe}\sqrt{(1\mp e^{-q_\parallel L})/2}$. For $q_\parallel=0$, only longitudinal modes (volume plasmon with $\omega=\omega_{pe}$) can be excited.

We shall focus on a reference case, with ion diffuseness $\sigma_i=0.3L_F$, and electron temperature $T_e=0.008T_F\simeq 300$ K. The perturbation is taken to be $\delta v=0.08v_F$. Three values of the film thickness will be investigated, $L=100L_F\simeq 118$ Å, $L=200L_F$, and $L=300L_F$. The value of $\delta v$ has been rescaled in order to have the same excitation energy for all film thicknesses (i.e., $\delta v$ must scale like $L^{-1/2}$).

For all cases, the computational box $L_{\max}$ is chosen to be $L_{\max}=L+200L_F$, i.e., we allow for an empty buffer zone of $100L_F$ on each side of the film. The electric potential is then set to zero at the boundaries of the computational box, as was discussed in Sec. II. We stress that the choice of such

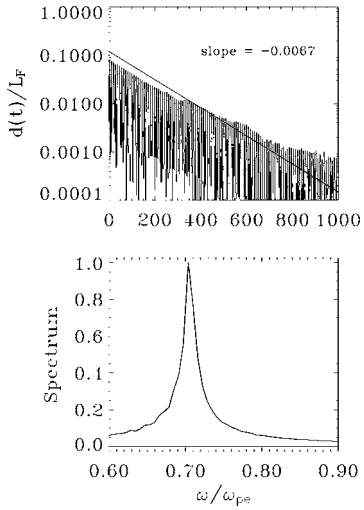


FIG. 8. Top, time history of the normalized electric dipole $d(t)/L_F$ on a semilog scale; the straight line is a fit to the numerical data. Bottom, frequency spectrum of the time history of the electric dipole, normalized to its maximum. Both figures refer to a film with $L=200L_F$.

boundary conditions is part of the physical problem under study and thus affects the linear response of the system, as was nicely shown by Hoh.[46] Therefore, typically linear quantities (like the oscillation frequency and damping rate of the electric dipole) may be quantitatively affected by the choice of the boundaries, though the qualitative picture remains the same. Nonlinear effects, such as the slow oscillations of the thermal energy described later, which are the main focus of the present paper, are only mildly affected by the choice of boundaries and are observed, with the same features, for all values of $L_{\max}$.

### A. Damping of the electric dipole

The relaxation of the electron gas is frequently studied by monitoring the evolution of the electric dipole,[22] defined as $d(t)=\int\int f_e x\,dx\,dv_x/\int\int f_e dx\,dv_x$. The dipole evolution is shown on a semilog scale in Fig. 8, together with its frequency spectrum, defined as the absolute value of the Fourier transform of $d(t)$.

The dipole oscillates at a frequency slightly smaller than the electron plasmon frequency and is initially damped exponentially with a rate approximately equal to $\gamma\simeq 0.0067\omega_{pe}$. The observed frequency is not exactly $\omega_{pe}$ because the computational box is necessarily finite (for example, we take $L_{\max}=300L_F$ for a film with $L=100L_F$). Indeed, it was shown[46] that the boundary conditions $\phi(\pm L_{\max})=0$ allow normal modes with a frequency less than $\omega_{pe}$. In a truly infinite medium ($L_{\max}\to\infty$), the fundamental frequency should approach $\omega_{pe}$, this point has been checked with our code by taking larger and larger computational boxes.

The observed value of the damping rate is also sensitive to the choice of the boundary conditions and therefore we do not attempt to derive a scaling law with the film thickness. Nevertheless, we stress that the same qualitative behavior

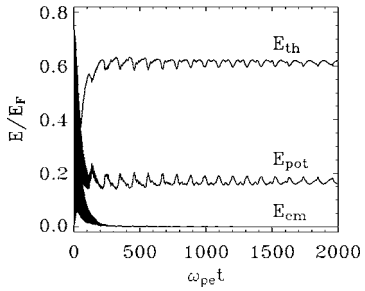


FIG. 9. Time evolution of the thermal, electric, and center-of-mass energies for a film thickness $L=100L_F$.

(exponential damping) has been observed for all choices of $L_{\max}$.

### B. Energy relaxation

The long-time electron relaxation is studied by following the time history of the energy quantities defined in Sec. IV. The kinetic energy is now decomposed into the sum of the Thomas-Fermi, thermal, and center-of-mass energies. The latter is defined as the kinetic energy of center of mass of the electron distribution, $E_{\text{c.m.}}=1/2\int[j_e^2(x,t)/n_e(x,t)]dx$ (where $j_e=\int v_x f_e dv_x$ is the electron current). Preliminary results on this issue were published in a previous paper.[33] Several phases can be identified in the time evolution (Fig. 9). An initial phase features damped collective oscillations of the electron gas occurring at a frequency close to $\omega_{pe}$, which correspond to the damping of the electric dipole discussed above. These fast oscillations are observed in the behavior of $E_{\text{pot}}$ and $E_{\text{c.m.}}$ up to $\omega_{pe}t\simeq 200$. At this time, the center-of-mass energy is almost entirely converted into thermal energy (kinetic energy around the Fermi surface). The Thomas-Fermi energy (not shown on the figure) remains almost unchanged during the entire run.

After saturation of the thermal energy at $\omega_{pe}t\simeq 200$, a slowly oscillating regime appears, with period $\approx 100\omega_{pe}^{-1}$. These slow oscillations are slightly damped, but still persist until the end of the run (the total duration of this run was $\omega_{pe}t=3000$). The oscillation period is roughly equal to the time of flight of electrons traveling through the film at a velocity close to the Fermi velocity of the metal. Therefore, we attributed this effect to nonequilibrium electrons bouncing back and forth against the surfaces of the film. In order to test this hypothesis, we have simulated two other films with different thicknesses, $L=200L_F$ and $L=300L_F$. The results are plotted in Fig. 10 and confirm that the oscillation period scales linearly with the film thickness. The propagation velocity across the film can be estimated to be very close to $v_F$.

Similar low-frequency oscillations were recently measured in transient reflection experiments on thin gold films, where it was also observed that their period is proportional to the thickness of the film.[47] The explanation provided by the authors is basically identical to our interpretation of the present numerical results.

The above simulations have highlighted two important facts, (i) electron transport is ballistic and occurs at a velocity close to $v_F$, in agreement with experimental measurements in thin gold films;[1,2] (ii) electron-surface interactions play an important role in the dynamical processes, which was not unexpected, since the thickness of the slab is smaller than the electron mean free path (equal to 340 Å for bulk sodium[30]).

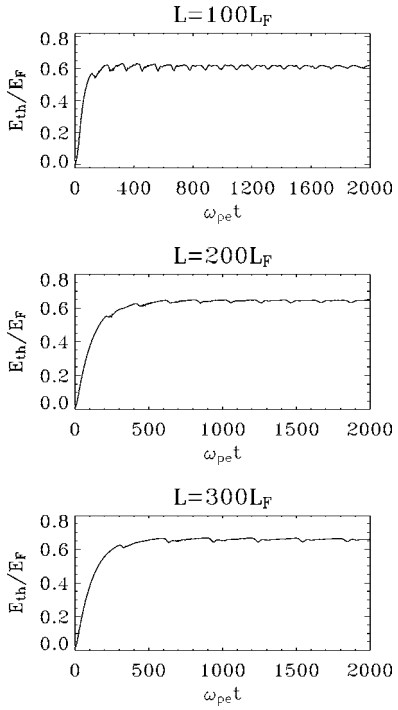


FIG. 10. Time evolution of the thermal energy for three values of the film thickness, $L=100L_F$ (top), $L=200L_F$ (middle), and $L=300L_F$ (bottom).

In order to check that the above findings do not depend crucially on the electron temperature, we have repeated our reference run ($L=100L_F$) with initial temperature $T_e=0.08T_F\simeq 3000$ K (i.e., 10 times higher than before). The time history of the thermal energy (Fig. 11) is virtually identical to that observed in the low-temperature case, except for a trivial shift of the curve corresponding to the initially higher temperature. We have also checked that the same behavior does not depend on the ion density profile, by chang-

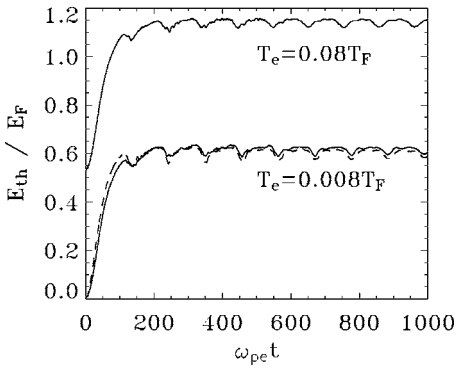


FIG. 11. Time evolution of the thermal energy for $\sigma_i=0.3L_F$ and initial temperatures $T_e=0.008T_F$ and $T_e=0.08T_F$ (solid lines) and for $\sigma_i=L_F$ and $T_e=0.008T_F$ (dashed line). The film thickness is $L=100L_F$.

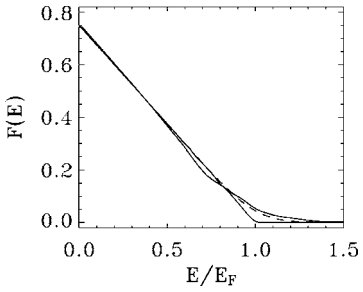


FIG. 12. Solid lines, energy distribution functions at $t=0$ and $\omega_{pe}t=3000$ for a film with $L=100L_F$ and initial temperature $T_e^{\text{init}}=0.008T_F$. The dashed line represents an analytical Fermi-Dirac distribution with temperature $T_e^{\text{final}}=0.0863T_F$.

ing the diffuseness parameter to $\sigma_i=L_F$ (instead of the previously used $\sigma_i=0.3L_F$). The result is also plotted in Fig. 11 and shows little variation in the thermal energy evolution. We conclude that the observed behavior is robust over a wide range of temperatures (at least as long as the electron gas remains fully degenerate) and for different ion density profiles.

The energy distribution at $\omega_{pe}t=3000$ [computed from Eq. (7)] is displayed in Fig. 12 for the run with $L=100L_F$ (qualitatively similar results were obtained for the other cases). For the sake of comparison, a Fermi-Dirac distribution with temperature $T_e^{\text{final}}=0.0863T_F$ is also plotted on the same graph. This final temperature is obtained from the thermal energy of the electron distribution at the end of the run, using the bulk estimate $\bar{E}_{\text{th}}/E_F=(\pi^2/12)(T_e/T_F)^2$. Clearly, the electron gas has evolved toward a quasiequilibrium state characterized by an energy distribution close to a Fermi-Dirac function, with a temperature higher than the ground state. We note that this quasiequilibrium has been attained even though no electron-electron collisions were included in the model, the relaxation was entirely due to the Coulomb mean field.

The fine resolution of the Eulerian code allows us to investigate in detail the microscopic electron dynamics in the relevant phase space. The electron distribution function in phase space $f_e(x,v_x,t)$ is shown in Fig. 13, for the film with $L=100L_F$. The perturbation propagates coherently from surface to surface with a speed close to the Fermi velocity. For instance, at $\omega_{pe}t=50$, the front of the perturbation (small bump on the outer contour in Fig. 13) has almost reached the point $x=0$; the small delay corresponds to an initial phase shift of half a period $\pi/\omega_{pe}$. Coherent structures (vortices) are indeed observed around the phase space region near $v_F$ (see the zoom in Fig. 14 at $\omega_{pe}t=50$). The vortex size is of the order of $2\pi L_F$ (which corresponds to a wave number $qL_F=1$) and does not depend on the film size. These structures correspond to nonequilibrium electrons being trapped in the propagating wave and are known to appear in wave-particle interactions in classical plasmas.[48] When the perturbation reaches the opposite surface, it is reflected back and interacts with the rest of the nonequilibrium electrons, thus inducing a loss of the coherence (i.e., vortices are destroyed). After several collisions with the surfaces, most of the nonequilibrum electrons are spread in a region around the Fermi surface (see Fig. 14 at $\omega_{pe}t=1000$), leading to a high-

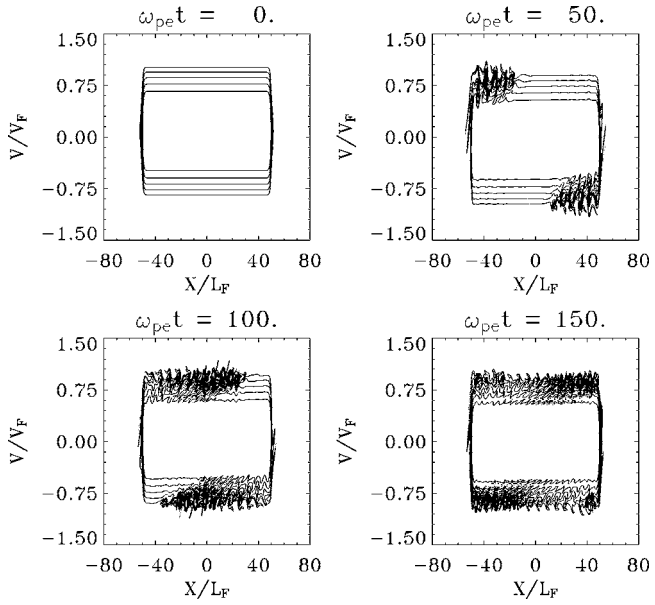


FIG. 13. Contour plots of the electron distribution function in phase space, at different instants, for a film thickness $L=100L_F$.

temperature quasiequilibrium state with a Fermi-Dirac energy distribution, as was shown in Fig. 12. Nevertheless, such mean-field thermalization is not quite complete, as the final energy distribution is not exactly a Fermi-Dirac one and some periodic oscillations still persist (Fig. 9).

### C. Effect of excitation energy

It is also interesting to analyze how the electron gas responds to different excitations energies. The excitation en-

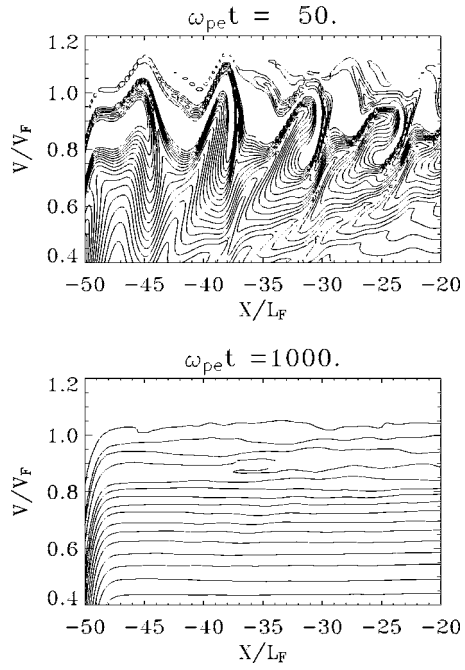


FIG. 14. Contour plots of the electron distribution function in phase space at $\omega_{pe}t=50$ and $\omega_{pe}t=1000$, for the film with $L=100L_F$ (same as Fig. 13). This plot shows a zoom near the Fermi surface.

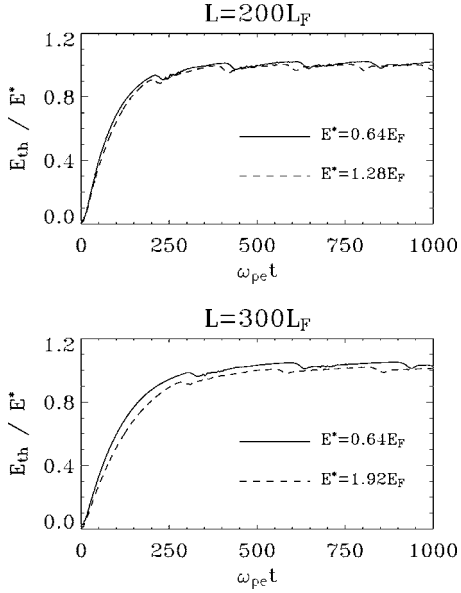


FIG. 15. Time evolution of the thermal energy, normalized to the excitation energy $E^*$, for different values of $E^*$. Top frame, $L=200L_F$; bottom frame, $L=300L_F$.

ergy per unit area $E^*$ is linked to the perturbation in velocity space $\delta v$ in the following way: $E^*/E_F=n_0L(\delta v/v_F)^2$. In the simulations shown in the preceding paragraphs, the value of $\delta v$ was rescaled ($\delta v \propto L^{-1/2}$) in order to have the same excitation energy for all film thicknesses, $E^*=0.64E_F$.

Now, we perform simulations corresponding to different excitation energies for several values of the film thickness. Figure 15 shows the evolution of the thermal energy, normalized to the excitation energy, for two values of $L$. For each case, the curves are almost exactly superimposed, which means that the increase in thermal energy scales linearly with the excitation energy, at least in the range considered here. This self-similar behavior is also in agreement with experimental measurements on thin gold films.[47]

## VI. ELECTRON-ION COUPLING

The results presented in the preceding sections were based on the assumption that, due to their large mass, the ions respond so slowly that they can be assimilated to a motionless, positively charged density (jellium model). However, for time scales of the order of a few hundred femtoseconds, or even shorter, the ions will start reacting to the electron motion, so that the above jellium model becomes no longer valid. For a correct treatment of the electron-ion coupling, one should, in principle, adopt a molecular dynamics point of view, and follow the (classical) trajectory of each ion. Some interesting results can nevertheless be obtained by supposing that the ions evolve in the same mean field as the electrons.

Here, we shall focus our attention on alkali metals, and more specifically sodium films, for which the influence of the core electrons can be neglected.[49] The ion dynamics is modelled via a Vlasov equation analogous to Eq. (1),

$$\frac{\partial f_i}{\partial t}+v_x\frac{\partial f_i}{\partial x}-\frac{e}{m_i}\frac{\partial \phi}{\partial x}\frac{\partial f_i}{\partial v_x}=0, \tag{8}$$

where $m_i=42\,228m_e$ is the mass of sodium ions.

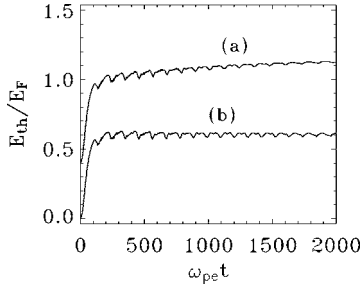


FIG. 16. Time evolution of the total thermal energy in the mobile ions case (a) and the fixed ions case (b). The film thickness is $L=100L_F$.

As the ions are classically distributed, their initial condition is given by a Maxwell-Boltzmann equilibrium

$$f_i(x,v_x,t=0)=\frac{n_i(x)}{\sqrt{2\pi T_i}}\exp\left(-\frac{m_iv_x^2}{2T_i}\right), \tag{9}$$

where the initial ion density $n_i(x)$ is defined in Eq. (3), and the ion temperature $T_i$ is taken to be equal to the electron temperature, $T_i=T_e=0.008T_F$. The initial electron distribution is obtained self-consistently in the same fashion described in Sec. V. (We note that the resulting ion-electron initial state is not, strictly speaking, a stationary solution of the Vlasov-Poisson system, though it becomes so in the limit $m_i\to\infty$.)

The inclusion of the ion dynamics does not alter the main conclusions drawn in the preceding sections. In particular, we still observe the initial Landau damping of the electric dipole and the propagation of the perturbation at a velocity close to the Fermi velocity.

The thermal energies for the fixed and mobile ions runs are shown in Fig. 16. In the mobile ions case, the electron density changes significantly, so that the Thomas-Fermi part of the kinetic energy is no longer approximately constant (as it was in the fixed ions runs). For this reason, we now define the electron thermal energy as $E_{\mathrm{th},e}=E_{\mathrm{kin},e}-E_{\mathrm{c.m.},e}-E_{\mathrm{TF}}(t=0)$ [it was defined as $E_{\mathrm{th},e}=E_{\mathrm{kin},e}-E_{\mathrm{c.m.},e}-E_{\mathrm{TF}}(t)$ in the fixed ions runs]. For the ions, the thermal energy is simply the kinetic energy, as the center of mass of the ion distribution is virtually motionless. The total thermal energy is given by the sum of the ion and electron components. The latter quantity is plotted in Fig. 16, together with the fixed ions result for comparison. The low frequency oscillations are still observed, but decay somewhat more quickly than in the fixed ions case. This is not unexpected, as the coupling to the ion dynamics provides an additional channel for dissipation.

It is also interesting to study the evolution of the ion and electron kinetic energies, which are shown in Fig. 17 for a film thickness $L=100L_F$. The plots show that the ions gain kinetic energy at the expense of the electron population. However, this process is considerably slower, and the electrons are still substantially more energetic than the ions at the end of the run.

The phase space portrait of the ion distribution function (Fig. 18) reveals that the electron-ion energy exchange is localized at the surfaces of the film,[12] where the ions are

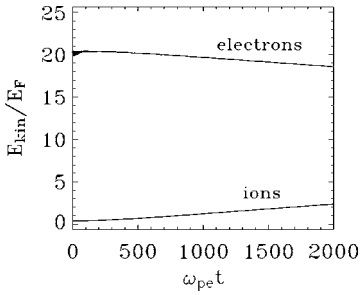


FIG. 17. Time evolution of the ion (a) and electron (b) kinetic energies. The film thickness is $L=100L_F$.

accelerated to velocities much larger than their initial thermal speed $\sqrt{k_B T_i/m_i} \simeq 3\times 10^{-4} v_F$. We stress again that the electron-ion coupling observed here is due to the mean field alone via Poisson's equation.

## VII. ELECTRON-ELECTRON COLLISIONS

The simulations presented in the preceding sections included only the mean field, but neglected the effect of electron-electron ($e$-$e$) collisions. This approximation is valid for short times, when the collisions have not yet been able to play a role, but should eventually break down on a longer time scale. In particular, the slow oscillations observed in Fig. 9 are expected to be damped by $e$-$e$ collisions whose characteristic time is much shorter than the oscillation period.

In order to assess the impact of $e$-$e$ collisions on the nonlinear dynamics, we make use of a simple relaxation model based on Landau's Fermi liquid theory. To model $e$-$e$ collisions, the right-hand side of the Vlasov equation (1) is now set to

$$\left(\frac{\partial f_e}{\partial t}\right)_{\text{coll}} \equiv -\nu_{ee}(T_e)(f_e - f_e^{\infty}), \tag{10}$$

where $\nu_{ee}$ is the average $e$-$e$ collision rate and $f_e^{\infty}(x,v_x)$ is a Fermi-Dirac distribution. The rationale behind this model is that the electron distribution will eventually relax towards a Fermi-Dirac equilibrium under the action of $e$-$e$ collisions, on a time scale of the order $\nu_{ee}^{-1}$. In order to select such equilibrium distribution $f_e^{\infty}$, we note that the electron cloud is supposed to be isolated from its environment (we neglect electron-ion couplings at this stage), so that the total energy is conserved. Therefore, $f_e^{\infty}$ can only be given by the Fermi-Dirac distribution which has total energy equal to that of the initial electron distribution $f_e(x,v_x,t=0)$ (including, of course, the initial excitation energy). In other words, we suppose to work in the microcanonical ensemble and require that $f_e$ relaxes to thermodynamic equilibrium under the constraint of total energy conservation.

The above prescription allows us to compute unambiguously $f_e^{\infty}(x,v_x)$. A minor caveat is that the latter is defined in terms of its temperature $T_e^{\infty}$, which needs to be computed from the total energy. This is done numerically by trial and error until a sufficient precision is obtained.

For electrons near the Fermi surface, the $e$-$e$ collision rate can be written as[21]

$$\nu_{ee}(T_e) = aT_e^2, \tag{11}$$

where $a$ is a (dimensional) proportionality constant. The latter has been estimated from numerical simulations of the electron dynamics in sodium clusters,[50] yielding $a \simeq 0.4\ \text{fs}^{-1}\ \text{eV}^{-2}$, which is also compatible with the analytical prediction given by the random phase approximation.[21]

In our simulations, we shall use a temperature-dependent collision rate, where $T_e$ is the instantaneous electron tem-

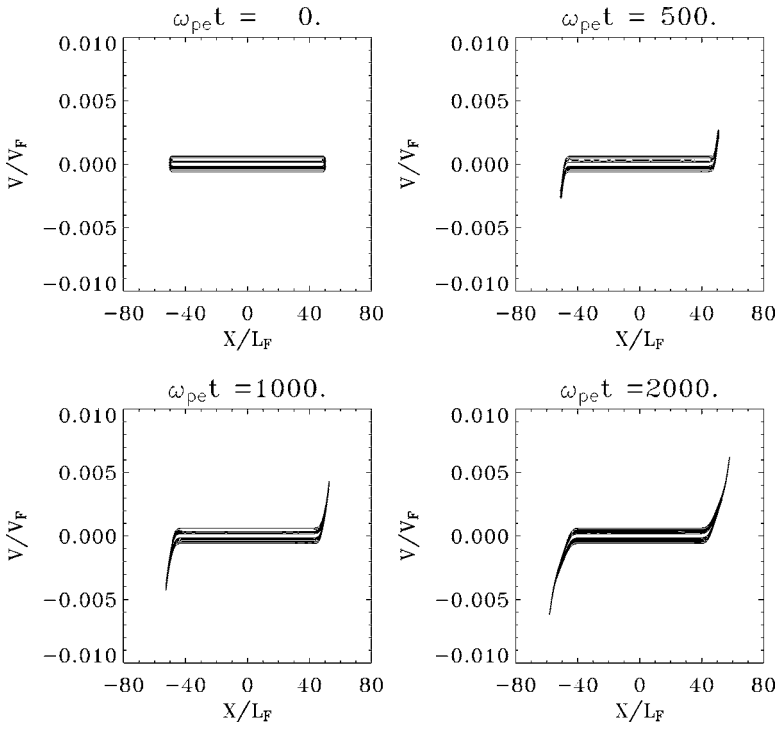


FIG. 18. Contour plots of the ion distribution function in phase space, at different instants, for a film thickness $L=100L_F$.

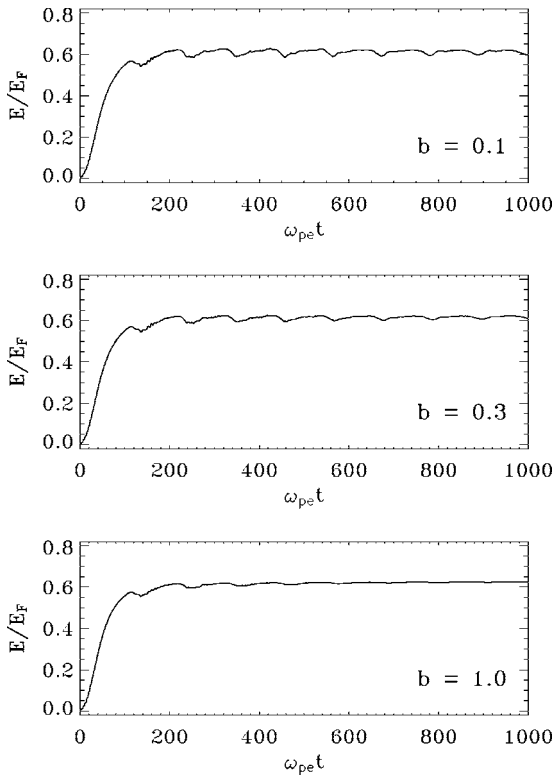


FIG. 19. Time evolution of the electron thermal energy for a case with *e-e* collisions and three different values of $b$. The film thickness is $L=100L_F$.

perature computed from the thermal energy per particle according to the bulk formula ($E_{\mathrm{th}}/N \propto T_e^2$) given in Sec. IV. The collision rate can thus be expressed in the nondimensional form,

$$\frac{\nu_{ee}}{\omega_{pe}} = \frac{b}{2}\frac{E_{\mathrm{th}}}{NE_F}. \tag{12}$$

Intuitively, the thermal energy is a good estimate of the portion of phase space that is open and thus available for collisions. For Eqs. (11) and (12) to be consistent, the dimensionless constant $b$ must take a value that is very close to unity, as can be easily shown by employing the physical parameters given in Sec. II for sodium. Nevertheless, in the numerical simulations, we will show results for various values of $b$, in order to highlight the effect of *e-e* collisions with respect to the purely mean-field dynamics.

We note that our model for *e-e* collisions, though fairly simple, does not rely on any free parameters and is entirely determined by fundamental considerations.

In Fig. 19, we show the evolution of the thermal energy for the reference case of a film of thickness $L=100L_F$ (see Fig. 9), for different values of $b$. The initial perturbation is $\delta v=0.08v_F$, which implies that the system must relax to a Fermi-Dirac distribution $f_e^\infty$ with temperature $T_e^\infty \simeq 0.086\,85T_F$ (note that this value is compatible with that of Fig. 12). For the realistic value $b=1$, the slow nonlinear oscillations are damped after a time $\sim 500\omega_{pe}^{-1} \simeq 50$ fs. Note

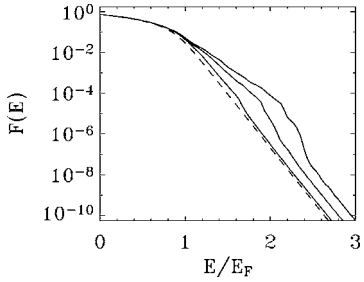


FIG. 20. Energy distribution function at $\omega_{pe}t=1000$, for the three cases of Fig. 19, $b=0.1$, $b=0.3$, and $b=1$. The dashed line is the analytical Fermi-Dirac equilibrium $f_e^\infty$ with temperature $T_e^\infty = 0.086\,85T_F$. The larger the value of $b$, the closer the curve is to the Fermi-Dirac equilibrium.

that the *e-e* damping time $\tau_{ee} \equiv \nu_{ee}^{-1}$ is approximately equal to $3.6\times 10^4 \omega_{pe}^{-1}$ at the start of the simulation (when $T_e = 0.008T_F$), but becomes $\omega_{pe}\tau_{ee} \simeq 330$ at saturation of the thermal energy. The latter value is consistent with the observed relaxation time.

Figure 20 shows the energy distribution function [see Eq. (7)] at $\omega_{pe}t=1000$, for three different values of $b$. For $b=1$, the distribution has virtually relaxed to the Fermi-Dirac equilibrium $f_e^\infty$, whereas for $b=0.1$ and $b=0.3$ some significant deviations from the equilibrium still persist.

A similar behavior is observed for a thicker film, $L = 200L_F$ (Fig. 21). As the collision rate scales as the inverse of the film thickness [as $N \sim L$ in Eq. (12)], the damping time is about twice as long in this case. The number of observed oscillation periods (which scales as $L$) is thus independent on the thickness of the film.

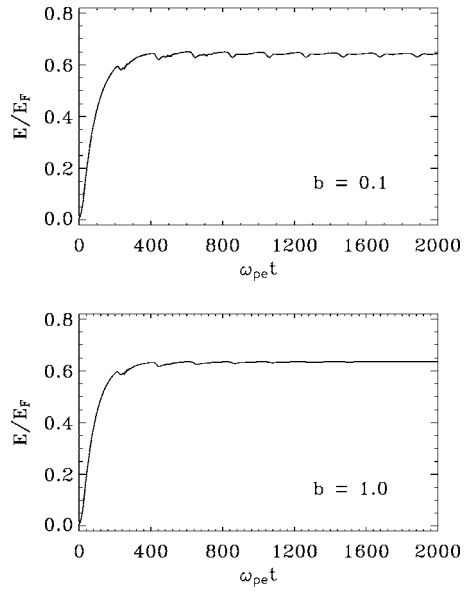


FIG. 21. Time evolution of the electron thermal energy for a case with *e-e* collisions and two different values of $b$. The film thickness is $L=200L_F$.

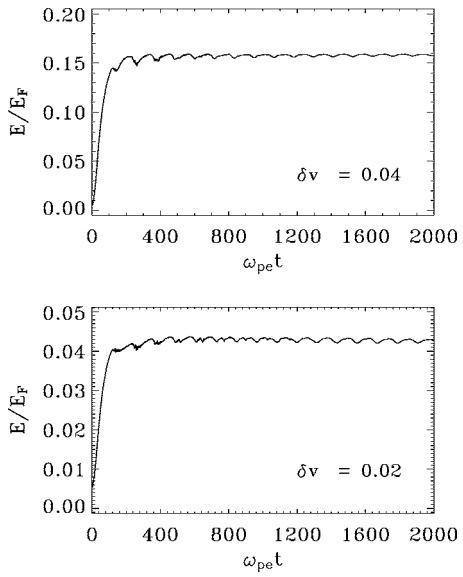


FIG. 22. Time evolution of the electron thermal energy for a case with *e-e* collisions ($b=1$) and two different values of $\delta v$. The film thickness is $L=100L_F$.

The *e-e* collision rate is a function of the thermal energy of the electron population, which in turn depends on the excitation energy $E^* \sim \delta v^2$. Therefore, we expect the effect of *e-e* collisions to diminish for lower excitation energies. This conjecture has been tested by running two cases at $L=100L_F$, with $\delta v=0.04v_F$ and $\delta v=0.02v_F$ (previously, we had $\delta v=0.08v_F$), using the realistic value $b=1$ (Fig. 22). Clearly, the damping is less effective for lower excitation energies, in agreement with our conjecture. For $\delta v=0.02v_F$, the nonlinear oscillations are still present at $\omega_{pe}t=2000$. These results indicate that, for sufficiently low excitations, the slow nonlinear oscillations should be observed in spite of the thermalizing effect of *e-e* collisions.

## VIII. DISCUSSION

In this work, we reported numerical results on the ultrafast dynamics of electrons and ions in thin metal films. We used a semiclassical one-dimensional model (Vlasov-Poisson system), which incorporates the effect of the mean Coulomb field, but neglects electron-electron collisions (the latter were included at a later stage). The adopted geometry is appropriate to study volume excitations, although it does not describe surface modes. The relative simplicity of our model can actually be a conceptual asset, as it allows one to isolate and study physical effects that are solely due to semiclassical and mean field phenomena.

The Vlasov-Poisson model was solved numerically using a very stable and accurate scheme for the Vlasov equation. This enabled us to follow the electron dynamics over long times (well into the nonlinear regime), without being encumbered by the numerical noise that pollutes most test-particle simulations.

Given the success of the model in explaining previous experimental findings[1,2] (and in predicting effects that were unpublished when the model was developed[47]), it appears that electron transport in metal films can indeed, to a large extent, be described by purely semiclassical and mean-field physics. Of course, further investigations will be needed to analyze the impact of quantum-mechanical and collisional effects on the present results.

We first studied the properties of the ground state, obtained via a Thomas-Fermi-type approach. The principal aim here was to understand whether the standard bulk properties also apply to finite-size systems. Our results showed that they do apply, for instance, we verified that, at low temperatures, the thermal energy scales like $T_e^2$, with the correct proportionality constant; the chemical potential also follows the bulk result, up to temperatures of the order of $T_F$. Thus, the presence of surfaces does not seem to play a major role on the properties of the ground state, although, as we have seen, it is of paramount importance for transport phenomena.

Concerning the dynamical aspects of our study, previous experimental measurements on thin gold films[1,2] had suggested that electron transport is ballistic and occurs at a speed close to the Fermi velocity of the metal. Our numerical results confirmed both these conclusions, indeed, contour plots of the electron phase space distribution clearly showed that the transport is due to bunches of nonequilibrium electrons traveling through the film with a speed close to $v_F$.

By bouncing back and forth on the film surfaces, these electrons trigger a regime of slow oscillations in the thermal energy, with period equal to the time-of-flight $L/v_F$. This regime is not altered by changing the electron temperature, the ion density profile, or the initial excitation. After several collisions with the film surfaces, these electrons get smeared out on the Fermi surface, giving rise to an apparent temperature increase in the electron population. We stress that such heating effect is entirely due to mean-field interactions, electron-electron collisions having been neglected so far.

Including the ion mean-field dynamics did not change most of the above conclusions. It was observed that kinetic energy is gradually transferred from the electron to the ion population. This results in significant ion accelerations, localized at the surfaces of the film.

A simple (but parameter-free) model was devised in order to take into account the effect of electron-electron collisions. Although the collision term tends to damp the slow nonlinear oscillations, several oscillation periods were still observed. In addition, the collision term becomes less effective for smaller excitations, because a smaller portion of the phase space is opened up and thus available for collisions.

The present work could be generalized to take into account quantum-mechanical effects, by replacing the Vlasov equation with the Wigner equation.[51] Comparison with the present results would allow us to sort out typically quantum phenomena from the semiclassical dynamics treated here.

## ACKNOWLEDGMENTS

The authors would like to thank Jean-Yves Bigot for his invaluable suggestions and constant support. The numerical calculations were performed on the computers of the IDRIS computing center in Orsay, France.

[1] S. D. Brorson, J. G. Fujimoto, and E. P. Ippen, Phys. Rev. Lett. **59**, 1962 (1987).
[2] C. Suárez, W. E. Bron, and T. Juhasz, Phys. Rev. Lett. **75**, 4536 (1995).
[3] R. H. M. Groeneveld, R. Sprik, and A. Lagendijk, Phys. Rev. B **51**, 11433 (1995).
[4] G. L. Eesley, Phys. Rev. Lett. **51**, 2140 (1983).
[5] C.-K. Sun, F. Vallée, L. H. Acioli, E. P. Ippen, and J. G. Fujimoto, Phys. Rev. B **50**, 15337 (1994).
[6] J.-Y. Bigot, V. Halté, J.-C. Merle, and A. Daunois, Chem. Phys. **251**, 181 (2000).
[7] M. Bauer and M. Aeschlimann, J. Electron Spectrosc. Relat. Phenom. **124**, 225 (2002).
[8] W. Rudolph, P. Dorn, X. Liu, N. Vretenar, and R. Stock, Appl. Surf. Sci. **208-209**, 327 (2003).
[9] J-S. Lauret, C. Voisin, G. Cassabois, C. Delalande, Ph. Roussignol, O. Jost, and L. Capes, Phys. Rev. Lett. **90**, 057404 (2003).
[10] R. Schlipper, R. Kusche, B. v. Issendorff, and H. Haberland, Appl. Phys. A: Mater. Sci. Process. **72**, 255259 (2001).
[11] E. E. B. Campbell, K. Hansen, K. Hoffmann, G. Korn, M. Tchaplyguine, M. Wittmann, and I. V. Hertel, Phys. Rev. Lett. **84**, 2128 (2000).
[12] M. Nisoli, S. Stagira, S. De Silvestri, A. Stella, P. Tognini, P. Cheyssac, and R. Kofman, Phys. Rev. Lett. **78**, 3575 (1997).
[13] C. Voisin, D. Christofilos, N. Del Fatti, F. Vallée, B. Prével, E. Cottancin, J. Lermé, M. Pellarin, and M. Broyer, Phys. Rev. Lett. **85**, 2200 (2000).
[14] W. S. Fann, R. Storz, H. W. K. Tom, and J. Bokor, Phys. Rev. B **46**, 13592 (1992).
[15] B. Rethfeld, A. Kaiser, M. Vicanek, and G. Simon, Phys. Rev. B **65**, 214303 (2002).
[16] M. Aeschlimann, M. Bauer, S. Pawlik, R. Knorren, G. Bouzerar, and K. H. Bennemann, Appl. Phys. A: Mater. Sci. Process. **71**, 485 (2000).
[17] C. Voisin *et al.*, J. Phys. Chem. B **105**, 2264 (2001).
[18] R. Knorren, G. Bouzerar, and K. H. Bennemann, Phys. Rev. B **63**, 125122 (2001).
[19] C. Guillon, P. Langot, N. Del Fatti, and F. Vallée, New J. Phys. **5**, 13 (2003).
[20] F. Vallée, C. R. Acad. Sci., Ser IV: Phys., Astrophys. **2**, 1469 (2001).
[21] D. Pines and P. Nozières, *The Theory of Quantum Liquids* (Benjamin, New York, 1966).
[22] F. Calvayrac, P.-G. Reinhard, E. Suraud, and C. Ullrich, Phys. Rep. **337**, 493 (2000).
[23] Uwe Schwengelbeck, Luis Plaja, Luis Roso, and Enrique Conejero Jarque, J. Phys. B **33**, 1653 (2000).
[24] J. Daligault and C. Guet, J. Phys. A **36**, 5847 (2003).
[25] S. V. Fomichev and D. F. Zaretsky, J. Phys. B **32**, 5083 (1999).
[26] D. F. Zaretsky, Ph. A. Korneev, S. V. Popruzhenko, and W. Becker, J. Phys. B **37**, 4817 (2004).
[27] F. Filbet, E. Sonnendrucker, and P. Bertrand, J. Comput. Phys. **172**, 166 (2001).
[28] M. Madjet and P.-A. Hervieux, Eur. Phys. J. D **9**, 217 (1999).
[29] A. Kawabata and R. Kubo, J. Phys. Soc. Jpn. **21**, 1765 (1966).
[30] U. Kreibig and M. Vollmer, *Optical Properties of Metal Clusters* (Springer, New York, 1995).
[31] B. Lamprecht, J. R. Krenn, A. Leitner, and F. R. Aussenegg, Phys. Rev. Lett. **83**, 4421 (1999).
[32] R. A. Molina, D. Weinmann, and R. A. Jalabert, Phys. Rev. B **65**, 155427 (2002).
[33] G. Manfredi and P.-A. Hervieux, Phys. Rev. B **70**, 201402(R) (2004).
[34] N. W. Ashcroft and N. D. Mermin, *Solid State Physics* (Saunders College, Orlando, 1976).
[35] C. Jarzynski and G. F. Bertsch, Phys. Rev. C **53**, 1028 (1996).
[36] K. Morawetz and R. Walke, Physica A **330**, 469 (2003).
[37] A. Domps, A.-S. Krepper, V. Savalli, P.-G. Reinhard, and E. Suraud, Ann. Phys. **6**, 468 (1997).
[38] A. Domps, P.-G. Reinhard, and E. Suraud, Ann. Phys. (N.Y.) **260**, 171 (1997).
[39] C. Z. Cheng and G. Knorr, J. Comput. Phys. **22**, 330 (1976).
[40] T. D. Arber and R. G. L. Vann, J. Comput. Phys. **180**, 339 (2002).
[41] N. Besse and E. Sonnendrücker, J. Comput. Phys. **191**, 341 (2003).
[42] L. D. Landau and E. M. Lifshitz, *Statistical Physics*, Part 1 (Butterworth-Heinemann, Oxford, 1980).
[43] P.-A. Hervieux and J.-Y. Bigot, Phys. Rev. Lett. **92**, 197402 (2004).
[44] M. Anderegg *et al.*, Phys. Rev. Lett. **27**, 1565 (1971).
[45] A. Liebsch, *Electronic Excitations at Metal Surfaces* (Plenum, New York, 1997).
[46] F. C. Hoh, Phys. Rev. **133**, A1016 (1964).
[47] X. Liu, R. Stock, and W. Rudolph, *CLEO/IQEC and PhAST Technical Digest on CDROM* (The Optical Society of America, Washington, DC, 2004), IWA4.
[48] G. Manfredi, Phys. Rev. Lett. **79**, 2815 (1997).
[49] M. Breitholtz, T. Kihlgren, S.-Å. Lindgren, H. Olin, E. Wahlström, and L. Walldén, Phys. Rev. B **64**, 073301 (2001).
[50] A. Domps, P.-G. Reinhard, and E. Suraud, Phys. Rev. Lett. **81**, 5524 (1998).
[51] E. P. Wigner, Phys. Rev. **40**, 749 (1932).